Equally likely inverse solutions to a groundwater flow problem including pattern information from remote sensing images

H. J. Hendricks Franssen,[1] P. Brunner,[1,2] P. Makobo,[3,4] and W. Kinzelbach[1]

Received 8 April 2007; revised 2 October 2007; accepted 16 October 2007; published 17 January 2008.

[1] Groundwater flow modeling for large areas in arid and semiarid regions, like the Chobe region in Botswana, suffers from a severe lack of data. This study addresses the usefulness of remote sensing (RS) images to constrain the recharge rate estimates for a region. The estimates derived from METEOSAT and NOAA advanced very high resolution radar (AVHRR) images are correlated with recharge rate values estimated from chloride measurements and used jointly in the generation of multiple, equally likely recharge rate realizations with the colocated cosimulation algorithm. The colocated cosimulation algorithm is very suited to generate stochastic realizations of a parameter that includes information from a correlated covariable given on a regular, dense grid as in RS information. These equally likely recharge rate realizations, together with multiple equally likely transmissivity realizations, are conditioned by inversion to hydraulic head data and a digital elevation model. For the inverse conditioning an additional penalty term was added to the objective function, penalizing too large deviations of the recharge rate pattern from the RS image. As such, the recharge rate pattern observed with the RS images is still honored by the calibrated recharge rate realizations. It was observed that conditioning to the RS information reduces significantly the estimated ensemble variance of the recharge rates.

Citation: Hendricks Franssen, H. J., P. Brunner, P. Makobo, and W. Kinzelbach (2008), Equally likely inverse solutions to a groundwater flow problem including pattern information from remote sensing images, *Water Resour. Res.*, *44*, W01419, doi:10.1029/2007WR006097.

1. Introduction

[2] Numerical groundwater flow models have to deal with large uncertainties due to uncertain values of the input parameters. Traditionally, in models for humid regions a strong emphasis is placed on the uncertainty of hydraulic conductivity, which may vary over many orders of magnitude in a relatively small region, while recharge is known much better. Especially for the prediction of the transport of contaminants in an aquifer, detailed information on the spatial distribution of hydraulic conductivities is important. Typical applications where hydraulic conductivities are of great importance are the assessment of the transport of contaminants, the protection of well capture zones [e.g., *Stauffer et al.*, 2005], and the design of nuclear waste repositories [e.g., *Seong and Rubin*, 1999]. In semiarid regions, groundwater flow modelers face even larger uncertainties than under humid conditions, due to the erratic nature of recharge. Contaminant transport modeling is usually not the aim in these areas, and very detailed knowledge of the spatial distribution of hydraulic conductivities is therefore not required. However, a special interest exists in the recharge rates, the knowledge of which is the basis for sustainable water management. Recharge rates in semiarid areas are subject to a much larger uncertainty than in humid climates for various reasons [e.g., *Lerner et al.*, 1990; *Scanlon et al.*, 2006].

[3] 1. Precipitation shows a high variability in space and time (a large part of precipitation is associated with deep convection, which acts on smaller length and time scales than, for example, the extratropical cyclones in the temperate, humid climates).

[4] 2. Recharge is associated with complicated interrelations between weather, vegetation density, and soil properties as actual evapotranspiration is in general soil-controlled.

[5] 3. Recharge can only occur in some specific locations and after rainfall events surpassing a threshold intensity (e.g., in local depressions after a period of intensive rainfall) [*Leduc et al.*, 1997].

[6] 4. Data on the processes that govern areal recharge (precipitation, wind speed, humidity, incoming short-wave radiation, soil and vegetation properties) are more scarce in semiarid regions, often situated in the developing world.

[7] 5. Recharge rates are very small, and a small absolute error in the recharge rate may propagate into an error of an order of magnitude when estimating sustainable yields. This stresses the need for alternative data sources in semiarid regions in order to improve groundwater flow modeling.

[8] Remote sensing (RS) images may provide important information to improve a model (see, e.g., *Becker* [2006] and *Brunner et al.* [2007] for an overview). However, remote sensing images do in general not directly map a

[1]Institute of Environmental Engineering, ETH Zurich, Zurich, Switzerland.
[2]Now at School of Chemistry, Physics and Earth Sciences, Flinders University, Adelaide, South Australia, Australia.
[3]Department of Water Affairs, Gaborone, Botswana.
[4]Deceased 11 June 2006.

0043-1397/08/2007WR006097

parameter of interest, but are more or less well correlated to such a parameter. Therefore, in the first place, ground control measurements are necessary in order to scale the remote sensing images to the variable of interest. In the second place, it is important to consider the uncertainty of the remote sensing image in the groundwater modeling procedure. Ground control measurements can also be of help to estimate the error statistics of the remote sensing data. The uncertainty of the remote sensing images has to be weighted against the uncertainty of other data sources and information involved in the modeling procedure. In the modeling of land-surface processes and the estimation of, for example, spatial soil moisture contents or evaporative fluxes, the integration of remote sensing data into models in a statistical sense is an important research topic. Data assimilation techniques like ensemble Kalman filtering or variational algorithms are used to combine, for example, microwave-derived soil moisture estimates, soil moisture measurements, and predictions from land-surface models to obtain an analysis of the spatial distribution of the required parameter [e.g., *Margulis et al.*, 2002; *Boni et al.*, 2001; *Reichle et al.*, 2001; *Crow and Wood*, 2003]. The weight for the different pieces of information depends on their covariance matrices. It is common in these model calibration studies to calculate a filter solution (like the ensemble Kalman filter), which is very well suited for real-time modeling, incorporating sequentially new data that are continually measured or monitored. Also, a batch of observations from multiple observation times can be used in the ensemble smoother approach [*Dunne and Entekhabi*, 2005].

[9] In this paper, however, we address a different problem. Here remote sensing images are used to estimate an average recharge rate, which means a recharge rate that is averaged over many years. Therefore the data are not incorporated sequentially into a transient model, but all at once into an averaged steady state model, which can be done by some form of inverse modeling. In addition, although a model and different data sources are combined, and each has an uncertainty, it can be stated that the hydraulic head measurements have a much smaller uncertainty compared with the uncertainty of model input parameters such as transmissivity and recharge rate. Consequently, the uncertainty is dominated by the unknown spatial distributions of both areal recharge and transmissivity. Therefore, in order to improve the groundwater flow model, the focus lies on the improved characterisation of both the spatially variable transmissivities and recharge rates. Because an overestimation of the piezometric head can be corrected by both reducing the recharge rate and increasing the transmissivity, a crucial question is how to estimate transmissivities and recharge rates jointly in a satisfactory way.

[10] *Hendricks Franssen et al.* [2004] extended a method for the stochastic inverse modeling of groundwater flow, the sequential self-calibrated method (SSC) [*Gómez-Hernández et al.*, 1997; *Hendricks Franssen*, 2001], to the joint estimation of transmissivities and recharge rates. It was illustrated that in the case of sufficient prior information, good results can be obtained. This approach is also used in this study, simultaneously conditioning to transmissivity data, hydraulic head data, and recharge estimates from chloride data. However, the method up to now could not include the exhaustive (spatial pattern) information on transmissivities and/or recharge rates in the inverse modeling in a satisfying way. Some methodologies exist that can handle exhaustive soft information in inverse modeling to some extent. *Oliver et al.* [1997] constrain the variogram of the parameter of interest (in their case hydraulic conductivity) in the inverse modeling procedure. If the variogram is estimated on the basis of exhaustive soft information, it makes sense to preserve this measure of spatial continuity in the subsequent model calibration. However, it does not preserve the full information potential of the remote sensing image as it only considers area-averaged two-point statistics. A more rigorous approach to include exhaustive soft information is the method of conditional probabilities, proposed by *Capilla et al.* [1999]. In this methodology, exhaustive soft information is included in the SSC by perturbing the conditional probabilities (conditioned to the exhaustive soft information as well) instead of perturbing directly the values for the parameter of interest. This approach also has some drawbacks: A large number of indicator variograms have to be inferred, and the indicator variograms are area averaged two-point statistics. In addition, the perturbation of the image is only constrained by the inferred univariate local conditional probability density functions. More recently, *Kowalsky et al.* [2004] proposed a method to include geophysical measurements in an inversely conditioned flow model for the unsaturated zone, on the basis of a maximum a posteriori likelihood (MAP) formulation of the pilot point method [*LaVenue et al.*, 1995]. However, *Kowalsky et al.* [2004] do not explain how the weighting of the different pieces of information was carried out.

[11] An additional piece of soft information integrated into the groundwater flow simulations was a digital elevation model (DEM). If no artesian conditions are observed in an area, the groundwater heads should be below the terrain. For remote areas with few hydraulic head measurements, but with a DEM, such information can be used to additionally constrain the groundwater flow model.

[12] This paper presents an extension of the SSC to incorporate exhaustive soft information from RS. A difference with respect to the methods mentioned above is that the conditioning focuses on the use of the pattern information from the RS image for the model calibration. The availability of the exhaustive information puts additional constraints on the calibration of the input parameters of the groundwater flow problem.

2. Methodology

[13] The approach that is followed in conditioning to exhaustive RS data consists of multiple steps that are described in more detail below. It is assumed that the recharge rates (i.e., recharge on a pixel-wise basis) are estimated from RS data.

2.1. Generating Equally Likely Conditional Realizations

[14] Equally likely realizations of the parameters, needed as input to the groundwater flow equation, are generated. These equally likely realizations are conditioned to the available measurements with geostatistical simulation techniques. In case only local measurements are available,

conditional realizations are generated with the sequential simulation algorithm GCOSIM3D [*Gómez-Hernández and Journel*, 1993]. If besides local measurements also RS data for an input parameter are available, they are included by means of colocated cosimulation [*Almeida and Frykman*, 1994]. For colocated cosimulation only one extra parameter has to be supplied (compared with the sequential simulation of a multi-Gaussian distributed variable): the linear correlation coefficient between the primary and the secondary variable. This linear correlation coefficient between the primary variable (in this study the recharge rate) and the secondary variable (the RS information) is normally based on a ground-truth campaign. The better the correlation, the more the spatially variable realizations generated by colocated cosimulation will resemble the pattern from the RS image. Therefore the generation of equally likely realizations, conditioned to RS information but not conditioned to information on the state variables, is relatively straightforward.

2.2. Definition of an Objective Function Not Accounting for Pattern Information

[15] The generated equally likely realizations are input to the numerical groundwater flow model which calculates the hydraulic head as a function of space and time. The objective function is calculated according to the common definition:

$$J = \left(h^{meas} - h^{sim}\right)^T C_{hh}^{-1} \left(h^{meas} - h^{sim}\right) + \Psi_Y \left(Y^{prior} - Y^{sim}\right)^T C_{YY}^{-1} \left(Y^{prior} - Y^{sim}\right), \quad (1)$$

where J is the objective function, $\mathbf{h^{meas}}$ is a vector of size N_h that contains the measured hydraulic heads at the N_h measurement locations, $\mathbf{h^{sim}}$ is a vector of size N_h that contains the simulated hydraulic heads at the measurement locations (the simulated hydraulic heads are mapped to the observation locations with help of the matrix $\mathbf{H}$ of size $N_h \times N_{grid}$ where N_{grid} is the number of grid cells of the numerical model. This matrix $\mathbf{H}$ has for each measurement a summed contribution at its corresponding row equal to 1), the superscript T means transposed, and $\mathbf{C_{hh}}$ is the error covariance matrix of size $N_h \times N_h$ that contains the error covariances between all observations, and is normally set equal to the identity matrix (in that case, it is assumed that all measurements have the same expected measurement error variance, and there are no correlations between measurement errors in space). The second term penalizes the modification of the input parameters, $\mathbf{\Psi_Y}$ is a vector with weights assigned to the different input parameters, and serves to express the relative weight of the two different parts of the objective function, $\mathbf{Y^{prior}}$ is a vector of size N_{prior} containing the measured (or estimated) values at the N_{prior} measurement locations, $\mathbf{Y^{sim}}$ is a vector of size N_{prior} containing the simulated (calibrated) values at the measurement locations for the same parameters, and $\mathbf{C_{YY}}$ is the covariance matrix that contains the covariances between the different input parameters. In the SSC, $\mathbf{Y^{prior}}$ includes the measurement locations and the master blocks (for more details on the master blocks, see section 2.4). However, note that in the SSC, heavily penalized deviations from the prior values are omitted frequently, and the modification of the prior parameter values is constrained by limits that are related to the conditional univariate probability density functions (pdf's) estimated by kriging. *Alcolea et al.* [2006] stress the importance of including the second part of the objective function in the calibration.

[16] In SSC the objective function is minimized in an iterative fashion with respect to the optimization parameters. For normally distributed parameters, minimizing the objective function (equation (1)) is equivalent to maximizing the likelihood that the calibrated parameters are true, given the measurements.

[17] One possibility to include the RS information in the inverse modeling would be to consider the RS data as prior information (available at each grid cell) with a covariance matrix $\mathbf{C_{YY}}$, where the covariance matrix contains all the covariances for the recharge rate parameter. In addition, the modification of the recharge rate values would be penalized in the objective function with weights $\mathbf{\Psi_Y}$ depending on the estimated measurement error of Y (of the RS information), in comparison with the head measurement errors. However, remote sensing information often does not give a good estimate of the absolute values of a parameter, and penalizing the perturbation of the parameter field is therefore not the best option. On the other hand, RS information represents a pattern with some areas having a lower value for the recharge rate and others having a higher value, and we believe that this pattern contains the most valuable information for the model. Therefore we would like to condition on difference vectors, that is, the difference of the values estimated by RS for the recharge rate at two different locations.

2.3. Modifying the Objective Function to Include Pattern Information

[18] A matrix $\mathbf{D}$ can be constructed that contains the differences in recharge rates between all the grid cells and therefore has the dimensions $N_{grid} \times N_{grid}$. This matrix does not contain absolute differences, but only 0 and 1. If the recharge rate for a row element (a grid cell i) of matrix $\mathbf{D}$ is larger than the recharge rate for a column element (a grid cell j), the value is 1, and if the value is smaller, the assigned number is 0. The diagonal elements are assigned the value 0.5.

[19] The colocated cosimulation algorithm is now used to generate a large number of stochastic realizations of the matrix $\mathbf{D}$ (for the study presented in this paper, 1000). This is simply done by generating another large set of equally likely realizations of recharge rates by colocated cosimulation, conditioned to the RS information, and calculating for each of the realizations the matrix $\mathbf{D}$. The average matrix $\mathbf{D^{av}}$ is calculated over the complete ensemble of equally likely realizations of $\mathbf{D}$, and as a consequence, $\mathbf{D^{av}}$ has for each of its elements values between 0 and 1, which can be interpreted as the conditional probability that in a certain grid cell i the recharge rate is larger than the recharge rate in another grid cell j. Also, a measure of the ensemble spread of $\mathbf{D}$ can be established. For each realization a lumped measure of the difference between the pattern from the RS image and the pattern from the stochastic realization can be calculated:

$$\Theta^{real} = \sum_{ij} \left| D_{ij}^{real} - D_{ij}^{av} \right|, \quad (2)$$

where D_{ij} are elements in the lower triangle of the matrix $\mathbf{D}$, $\mathbf{D^{real}}$ is the calculated $\mathbf{D}$ matrix for a stochastic realization,

and $\mathbf{D}^{\mathbf{av}}$ is the ensemble averaged $\mathbf{D}$ matrix. The lumped scalar Θ^{real} measures to what extent the pattern of the stochastic realization deviates from the RS image. On the basis of the large number of calculated Θ^{real} (e.g., 1000), a pdf of Θ can be constructed, and statistics such as the variance of Θ can be calculated.

[20] For the equally likely realizations that have been generated with the colocated cosimulation algorithm, and conditioned to the RS information and possibly other measurements related to the parameters of interest, the matrix $\mathbf{D}$ and in addition Θ^{real} can be calculated. The new definition is as follows:

$$\begin{aligned} J = & \left(\mathbf{h}^{\mathbf{meas}} - \mathbf{h}^{\mathbf{sim}}\right)^T \mathbf{C}_{\mathbf{hh}}^{-1} \left(\mathbf{h}^{\mathbf{meas}} - \mathbf{h}^{\mathbf{sim}}\right) \\ & + \Psi_Y \left(\mathbf{Y}^{\mathbf{prior}} - \mathbf{Y}^{\mathbf{aim}}\right)^T \mathbf{C}_{\mathbf{YY}}^{-1} \left(\mathbf{Y}^{\mathbf{prior}} - \mathbf{Y}^{\mathbf{aim}}\right) \\ & + \boldsymbol{\delta}\Psi_\Theta \left(\boldsymbol{\Theta}^{real} - \boldsymbol{\Theta}_{0.90}\right)^2 \\ & \boldsymbol{\Theta}^{real} > \boldsymbol{\Theta}_{0.90} \rightarrow \delta = 1 \\ & \Theta^{real} < \Theta_{0.90} \rightarrow \delta = 0, \end{aligned} \tag{3}$$

where ψ_Θ is a weighting parameter and $\Theta_{0.90}$ is the 90% percentile of the Θ distribution (determined with 1000 realizations; for 10% of the realizations, $\Theta^{real} > \Theta_{0.90}$). The third term introduced in the objective function only has a contribution in case $\Theta^{real} > \Theta_{0.90}$, so only if the pattern deviates too much from the RS image does this term add a contribution to J. It does not make sense to punish patterns that are more close to the RS image ($\Theta^{real} \ll \Theta_{0.90}$) stronger: One could defend that on the basis of the ground-truth campaign, and the limited "trust" we have in the quality of the RS images, a tendency in the calibration process to come too close to the RS image, should also be punished. However, if one starts to perturb randomly the recharge rate, and evaluates Θ^{real}, one will find that it is unlikely that Θ^{real} decreases considerably. So in other words, if during inverse calibration Θ^{real} decreases to "unexpected" low values (i.e., becomes more like the RS image), it is unlikely that this happens by chance, and it is merely an indication that the individual realizations differed too much from the RS image (i.e., the measurement error of the RS image was overestimated). Therefore only large deviations from the RS image are punished. The estimated pdf for Θ^{real} can be used to define ψ_Θ, and it is recommended to experiment with multiple values. A possibility is also to set ψ_Θ equal to $\sigma_h^2/\sigma_\Theta^2$ in the philosophy of the maximum likelihood estimation, but we recognize that the minimization of J with the additional penalty term is a somewhat approximative and intuitive manner to include the RS information (as opposed to using a formulation like in (1)), as we believe that the most important RS information is contained in the pattern and not in the absolute values. The formulation according to (3) should guarantee that the pattern from the RS image, which was completely captured using the colocated cosimulation to generate multiple recharge rate realizations, is not severely deformed during the additional conditioning to state information.

[21] The methodology can be extended further to include higher-order information, like three-point statistics on the spatial pattern of the variable of interest. In that case, Θ would measure the difference in pattern between a stochastic realization and the RS image also in terms of three-point statistics.

2.4. Inverse Conditioning of Realizations

[22] After calculating the objective function value for each of the realizations according to (3), the objective function is minimized in the following steps:

[23] 1. The objective function is minimized by modifying (or calibrating) the spatially variable recharge rate and transmissivity fields. It is too CPU intensive to calculate the partial derivatives of the objective function with respect to each of the transmissivity and recharge rate values at the grid cells. Therefore a limited number of grid cells is selected at which the recharge rates and log-transmissivities are calibrated. These are the so-called master blocks. However, this does not mean that only the transmissivities and the recharge rates at the master blocks are updated. The optimized perturbations of transmissivity and recharge rate at the master blocks are later interpolated to the rest of the grid cells by means of ordinary kriging (see step 3). The partial derivatives of the objective function with respect to the log-transmissivities and recharge rates at the master blocks take into account this posterior interpolation to the rest of the grid cells as the kriging coefficients are already known. Detailed formulations for two-dimensional (2-D) steady state flow are given by *Gómez-Hernández et al.* [1997], and for more complex settings by *Hendricks Franssen* [2001]. A set of master blocks, preferably two or three per correlation range, are laid out on a regular grid, with a random starting point. The positions of the master blocks are modified during the iterative conditioning process.

[24] 2. The partial derivatives of the objective function with respect to the optimization parameters (the log-transmissivities and recharge rates at the master blocks) are contained in the gradient vector. This gradient vector is calculated efficiently with the help of adjoint state equations (detailed formulations given by *Hendricks Franssen* [2001]). By means of nonlinear optimization algorithms (in the minimization process steepest descent, Fletcher-Reeves conjugate gradients, Hestenes-Stiefel conjugate gradients, and Quasi-Newton are alternated), the updating direction is obtained from the gradient, and the objective function is minimized along the updating direction. The result from this minimization is a perturbation of the parameter values at the selected master blocks. The perturbation is constrained such that the local recharge rate cannot be larger (smaller) than the interpolated recharge rate plus (minus) 3 times the kriging standard deviation.

[25] 3. The optimized perturbations are interpolated with ordinary kriging to the rest of the grid cells, using the variogram that has been inferred from the measurement data. Note that in calculating the gradient of the objective function, the interpolation of the perturbations to the rest of the grid cells is taken into account. The objective function is calculated for the updated set of parameters, and in case convergence is achieved ($J < \varepsilon$; where ε is a user-defined value, below which the difference between measured and simulated hydraulic heads is thought to be acceptable), the iterative process stops. In case $J > \varepsilon$, steps 1–3 are repeated.

2.5. Influence of RS Data in the Conditioning Process

[26] To summarize, RS images play the following role in constraining the uncertainty band width of groundwater flow models calibrated with SSC:

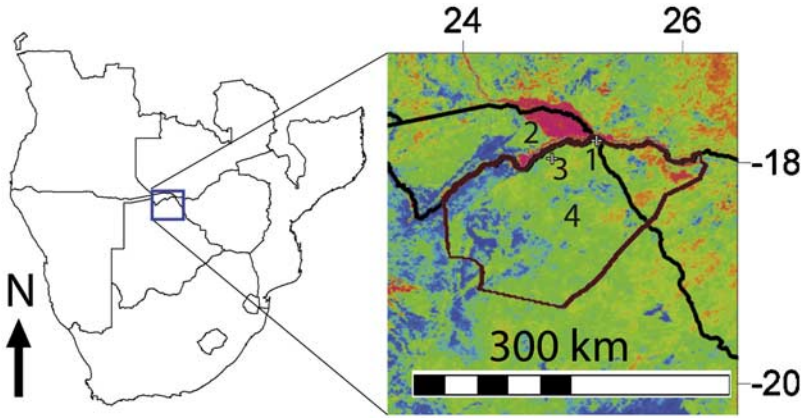

Figure 1. Location of the model area within southern Africa. The model area is indicated with brown lines around Kavimba. Numeral 1 corresponds to Kasane, 2 is the Chobe floodplain, 3 is Kavimba, and 4 is the forest reserve. Ngoma bridge is west of Kasane. The background map is an annual average of evapotranspiration. Red colors indicate a high evaporation rate, and blue colors indicate a low evaporation rate.

[27] 1. The estimated correlation length is more reliable due to the exhaustive RS data. The correlation length plays a role in generating the conditional recharge rate realizations, and in updating these relations in the conditioning to state information (interpolation of the optimised perturbations of the recharge rate).

[28] 2. Equally likely realizations of the recharge rate are generated by means of colocated cosimulation using recharge rate estimates at points (from chloride method) in combination with the exhaustive RS information. (These simulations are not yet conditioned to information on the state variables.)

[29] 3. In the inverse conditioning of the equally likely recharge rate realizations, the perturbation of the recharge rates is constrained by the univariate local pdf's, which have been estimated from all the data available, including RS data. The univariate local pdf's will be narrower due to the RS information.

[30] Steps 1–3 above do not guarantee that the inverse conditioned stochastic realizations honor the RS information. Therefore, in addition to 1–3,

[31] 4. The objective function is extended with an additional term that "measures" the modification of the spatial recharge rate pattern (compared with the RS image). The stronger the deviation, the larger the contribution to the objective function, making it more unlikely that for the conditioning to the hydraulic head data a solution is sought that has a spatial recharge rate pattern that deviates too much from the RS image.

[32] 5. In case we rely on recharge rate values estimated from the RS image (instead of the spatial pattern), and want to penalize the modification of these values during the inverse conditioning, equation (1) can be used, where the second term contains the recharge rate values estimated from the RS image $\mathbf{Y}^{\mathbf{prior}}$, and $\mathbf{Y}^{\mathbf{sim}}$ are the updated recharge rate values in the inverse conditioning. Note that in equation (1) the penalization of $\mathbf{Y}^{\mathbf{prior}} - \mathbf{Y}^{\mathbf{sim}}$ is weighted by the covariance matrix.

[33] In this paper, steps 1–4 are used to generate inverse realizations conditional to RS information, because it is believed that the RS pattern contains the important information, whereas the estimation of mean and variance (necessary for (5)) on the basis of RS images is associated with an important uncertainty.

3. Area Description and Problem

[34] The project area is the Chobe Forest Reserve in northern Botswana. Figure 1 shows the geographical location of the area.

[35] In 1998, the Department of Water Affairs in Botswana worked out several options for the future water supply of the Chobe Enclave villages Kavimba, Kachikau, Mabele, Parakarungu, and Satau. One of the options suggested was supplying the Chobe enclave with groundwater pumped in the Chobe Forest Reserve.

[36] To assess the feasibility of the future water supply by groundwater, a groundwater model was constructed. An important parameter related to the sustainability of this measure is groundwater recharge. This parameter has been assessed in a spatially distributed manner by combining remotely sensed data with chloride measurements on the ground [*Brunner et al.*, 2004]. The modeling approach showed that even with conservative recharge scenarios, the planned abstraction rates were far below groundwater recharge. However, independent of the modeling results, the water supply for the Chobe enclave is now provided through a pipeline bringing water from the nearby town of Kasane. Still, the aquifer in the Chobe region is one of the few untapped groundwater resources of Botswana. It therefore deserves special attention.

[37] The climate of the project area is semiarid with rainy, hot summers and dry winter seasons. In the project area, rainfall data are available for Kasane and for Kavimba, recorded as approximately 650 mm a^{-1} (Kasane). The daily mean air temperature varies between 16°C in winter (July–August) and 32°C in summer (November–December).

[38] The geology of the area is described as metamorphosed sediments, with intrusives of the Upper Proterozoic Ghanzi Group rock overlain by younger Stormberg lava of the Karoo Supergroup. Typical Stormberg Lava is a fine-grained crystalline, dark grey or purple-brown massive

Table 1. The Different Scenarios Studied

Scenario	Transmissivity Data?	Chloride Data?	Satellite Information?	Head Data?	Digital Elevation Model?	Patterns?
basis	yes	yes	no	no	no	no
h	yes	yes	no	yes	no	no
h + DEM	yes	yes	no	yes	yes	no
RS	yes	yes	yes	no	no	no
RS + DEM	yes	yes	yes	no	yes	no
RS + h	yes	yes	yes	yes	no	no
RS + h + DEM	yes	yes	yes	yes	yes	no
RS + h + Patt	yes	yes	yes	yes	no	yes
RS + h + DEM + Patt	yes	yes	yes	yes	yes	yes

Basalt rock. The enclave lies between two faults, the Shaile or Linyanti fault and the Kachikau fault. The Kachikau fault runs southwest from Ngoma Bridge through Mabele, Kavimba, and Kachikau. In Kavimba, Mabele, and Kachikau the fault separates the Chobe floodplain from the Chobe Forest Reserve which lies on a 70-m-higher plateau. Between Ngoma and Kavimba the Chobe River follows the Kachikau fault.

[39] In the project area the groundwater resources can be described by three units: the floodplain resources in the Kalahari Beds, the plateau resources in the Stormberg Lava, and the Kachikau fault line system in fracture zones. The Kachikau fault separates the resources in the floodplain and on the plateau. The hydraulic conductivity of the basalt depends on the grade of secondary porosity. The aquifers on the plateau and in the floodplain are unconfined. No artesian springs are present in the area. The aquifer is modeled by one aquifer layer. This may not be correct in places where the Kalahari sand cover becomes very thick (western part of the aquifer), and some of the water may be flowing in that formation rather than in the underlying basalt.

[40] The original, deterministic model contained a crude zonation of transmissivity. On the basis of the recharge map and the calibration of constant transmissivity for three different zones, the model was calibrated to steady state head data.

4. Description of Experiments

[41] For the area described in the previous section, a 2-D steady state groundwater flow model has been developed. The boundaries are mostly impervious, and at some parts prescribed heads are imposed. Close to the village of Kavimba, groundwater is pumped. Average long-term pumping rates have been imposed for six different wells. The area is discretized with the finite difference method in 215 × 125 grid cells of size 1059 m × 1102 m (corresponding to the resolution of a pixel of the RS images). Only part of this area belongs to the aquifer; the groundwater flow model has 14,437 active grid cells. The model setup and the pumping data were not modified in the process of model calibration and are considered deterministic.

[42] In a Monte Carlo approach, 100 equally likely inverse conditioned realizations have been generated. The parameters that are subject to uncertainty are transmissivity and recharge rate. For transmissivity, one set of 100 equally likely log-transmissivity (Y) realizations has been generated with sequential Gaussian simulation, implemented in the code GCOSIM3D [*Gómez-Hernández and Journel*, 1993]. The realizations are conditioned to six transmissivity measurements, and the mean Y differs slightly between the four different geological zones (including the Kachikau fault as one zone). The variogram of Y had to be postulated due to the limited number of measurement data. An exponential model has been chosen with an integral scale I_Y equal to 10 km and a sill σ_Y^2 equal to 0.25 $(\log_{10}(\mathrm{m}^2\ \mathrm{s}^{-1}))^2$, for all four zones. For all the simulations that are discussed below, the same set of 100 conditioned transmissivity realizations has been used as input.

[43] Nine different sets of 100 equally likely solutions to the inverse problem have been generated. Table 1 summarizes the different scenarios that have been studied. The scenarios are chosen such that the influence of RS data (*RS*), hydraulic head data (*h*), the digital elevation model (*DEM*) and the inclusion of pattern information (*Patt*) in the inverse modeling can be assessed.

[44] The influence of the RS data is investigated by generating two different sets of 100 equally likely recharge rate realizations. One set (used in scenarios *basis*, *h*, and *h + DEM*) is conditioned to the 16 recharge data (from the chloride measurements), and another set (used in scenarios *RS + DEM*, *RS + h*, *RS + h + DEM*, *RS + h + Patt*, and *RS + h + DEM + Patt*) is conditioned both to the 16 recharge data and the RS data. *Brunner et al.* [2004] detail how the recharge rate estimates from the 16 chloride data are obtained, how the precipitation estimate is obtained from METEOSAT5 images, and how the actual evapotranspiration is estimated from 47 NOAA images between 1990 and 2000. Here a short summary is given. The estimation of the precipitation (P) was based on the GOES Precipitation Index (GPI) algorithm [*Herman et al.*, 1997]. The estimation uses METEOSAT 5 images and rain gauge data. The spatial resolution is 8 km. The data were provided by the NOAA Climate Prediction Center for Famine Early Warning Systems and are available for download from http://www.cpc.noaa.gov/products/fews/data.html. Actual evapotranspiration (ET) estimates were based on NOAA14 images following a method suggested by *Roerink et al.* [2000]. The spatial resolution of the NOAA images was approximately 1 km. Actual evapotranspiration is the product of the average daily net radiation and the evaporative fraction. Following the method of *Roerink et al.* [2000], the evaporative fraction was extracted for each pixel of the satellite image by plotting all pixels of the image in a coordinate system of surface temperature versus ground albedo. Forty-seven NOAA images were processed according to this method. Principal component analysis of over 47

P-ET maps showed that the P-ET pattern in the project regions remained stable in time.

[45] The RS image that is used as a proxy for the recharge rate is a combination (precipitation − actual evapotranspiration) of these satellite images. The correlation between the RS images and the recharge obtained by using the chloride method is limited by both uncertainties of the RS approach and the chloride method. In addition, this approach neglects lateral flow between grid cells, which might play an important role depending on the topography. However, it is expected that in this relatively flat area lateral flow is not important. Also, cells are rather large and redistribution within a cell would not be relevant. Given the size of the cells, preferential recharge through fractures or macropores would still be occurring with a high frequency within one grid cell. All considered, we found a reasonably high correlation between the chloride measurements and the P-ET from the RS image. For the set that is only conditioned to the chloride measurements, equally likely recharge rate realizations with GCOSIM3D are built. It should be stated that the recharge rate variogram for those realizations was the same as estimated from the RS data, because the sparse chloride data did not allow for a meaningful variogram estimation. This means that for the case that chloride data are used in the conditioning procedure, but not a RS image, an unrealistically good variogram of the recharge rate is used. Therefore the worth of chloride data (in terms of improving the estimate and reducing the uncertainty) is expected to be slightly overestimated. The perturbation of the recharge rate realizations in the inverse modeling is only constrained by the maximum and minimum allowed local recharge rate values, which are set equal to the recharge rate estimated by lognormal kriging plus or minus 3 times the kriging standard deviation. The 100 equally likely realizations that are conditioned to both chloride measurements and RS data are generated with the colocated cosimulation algorithm, as explained in section 2. The estimated linear correlation coefficient between the recharge rate estimated from the chloride measurements and the recharge rate estimated from the RS data is 0.715 [*Brunner et al.*, 2004]. The parameters of the spherical recharge rate variogram were estimated from the RS data: 100 km for the integral scale I_R, 36 (mm a^{-1})^2 for the nugget, and 394 (mm a^{-1})^2 for the sill. The perturbation of these recharge rate realizations in the inverse conditioning is expected to be more strongly constrained because the kriging standard deviations are expected to be smaller. The kriging standard deviations are estimated with a colocated cokriging procedure, using both chloride measurements and RS data for the interpolation. In scenarios *RS*, *RS* + *DEM*, *RS* + *h*, and *RS* + *h* + *DEM* the perturbation of the recharge rate realizations in the inverse conditioning is only constrained by the maximum and minimum local recharge rate values. In scenarios *RS* + *h* + *Patt* and *RS* + *h* + *DEM* + *Patt* the perturbation of the recharge rate realizations is additionally constrained by pattern information. The distribution of Θ was estimated with the help of 1000 realizations. The matrix **D** used in equation (2) is calculated for a subset of 200 grid cells and has therefore dimensions 200 × 200. The subset of 200 grid cells is randomly located on the grid and varies from realization to realization. It is expected that the subset of 200 grid cells is large enough to capture the basic patterns of the RS data.

[46] In scenarios *h*, *h* + *DEM*, *RS* + *h*, *RS* + *h* + *DEM*, *RS* + *h* + *Patt*, and *RS* + *h* + *DEM* + *Patt* the realizations are inversely conditioned to the 22 steady state hydraulic head data. In the other scenarios these hydraulic head data are not used for conditioning. Field data collected suggest that the steady state assumption is justified. Hydraulic heads were monitored during a limited period (7 months) but nevertheless introduced as steady state, long-term average hydraulic heads in the model. In the monitoring period, which included important precipitation events, no significant variations in hydraulic head were recorded. More important, the groundwater levels were expected to be close to their long-term average in the zone. In addition, we did not calibrate the measured hydraulic head data very closely but tolerated differences of several meters. The calibration results indicated that the uncertainty with respect to the exact steady state head values had only a marginal impact on the estimated recharge rates. When inverse conditioning is performed, 600 master blocks are laid out on a regular grid with random starting point; 300 master blocks are for the optimization of the spatially variable transmissivities and 300 master blocks are for the optimization of the spatially variable recharge rates. The transmissivity is divided in four zones; the spatially variable transmissivities in each of the zones are perturbed independently.

[47] Finally, for some of the scenarios (scenarios *h* + *DEM*, *RS* + *DEM*, *RS* + *h* + *DEM*, and *RS* + *h* + *DEM* + *Patt*), information from a digital elevation model (DEM) is used to additionally constrain the inverse conditional realizations. The global digital elevation model GTOPO30 was used in this study. GTOPO 30 has a spatial resolution of 30 arc sec or approximately 1 km. (See also http://edc.usgs.gov/products/elevation/gtopo30/gtopo30.html.) The hydraulic head values calculated by the groundwater flow model should for each grid cell be lower than the altitude of the DEM, as there are no natural springs in the area. In order to achieve this, the objective function (defined according to (1) or (3)) is extended by an additional term that strongly penalizes point hydraulic head values that are more than 30.0 me above the (grid cell) terrain. The DEM we used still had an estimated error of the altitude around 5–6 m for a grid cell. Note that because we work with a relatively imprecise DEM, we can extract only limited information from it.

5. Results and Discussion

[48] For each of the scenarios, 100 equally likely solutions, conditioned to the different kinds of data, were generated. Ensemble statistics were calculated over these 100 realizations. The ensemble average transmissivity and recharge rate were computed for each active grid cell and in addition averaged over the model domain. The average ensemble standard deviation is evaluated as

$$AESD(X) = \frac{1}{N}\sum_{i=1}^{N}\sigma_{X_i}, \tag{4}$$

where X is recharge rate, transmissivity, or hydraulic head, N is the number of active grid cells and σ_{Xi} is the ensemble

Table 2. Evaluation of the Ensemble Statistics for the Studied Scenarios[a]

Scenario	Average Y, $\log(m^2\ s^{-1})$	$AESD(Y)$, $\log(m^2\ s^{-1})$	Average R, mm a^{-1}	$AESD(R)$, mm a^{-1}	$AESD(h)$, m
basis	−3.53	0.45	19.8	12.8	916.3
h	−2.42	0.72	9.8	8.6	665.9
h + DEM	−2.36	0.71	6.5	8.0	16.0
RS	−3.53	0.45	13.8	9.0	3083.6
RS + DEM	−1.71	0.68	6.0	4.0	6.4
RS + h	−2.31	0.74	9.0	5.4	454.3
RS + h + DEM	−2.38	0.61	6.4	3.3	10.3
RS + h + Patt	−2.29	0.72	8.5	5.2	244.3
RS + h + DEM + Patt	−2.25	0.67	6.9	4.3	11.2

[a] Y is log-transmissivity, R is recharge rate, h is hydraulic head, and $AESD$ is average ensemble standard deviation.

standard deviation for recharge rate, log-transmissivity, or hydraulic head for an active grid cell *i*. Table 2 displays the results for the different scenarios. Figure 2 shows the estimated ensemble average recharge rate over the area for the different scenarios.

[49] Scenario *basis*, based on log-transmissivity and chloride measurements only, without any other information, gives hydraulic head values that are too high compared with the measured values in large parts of the study area. In addition, the hydraulic heads are in some parts of the area far above the surface (while in reality no artesian conditions are observed). Some extremely high hydraulic head values in some of the realizations, cause the elevated $AESD(h)$ value. Because the value for $AESD(h)$ is strongly determined by some outliers with extremely high hydraulic head values, the estimate of $AESD(h)$ was not stable after 100 realizations. Many more realizations would have been needed. However, as it is evident that these realizations with extremely elevated hydraulic head values do not make sense, it is not interesting to stabilize their estimates.

[50] In scenarios *h* and *h + DEM* besides log-transmissivity data, also information on the hydraulic head values was used for conditioning. In scenario *h* only point hydraulic head measurements are used. The ensemble statistics show that an increased mean log-transmissivity and a reduced mean recharge are obtained, in order to reduce the excess piezometric head levels seen in the *basis* scenario. Nevertheless, in parts of the area the calculated piezometric head values are still above the soil surface (elevated $AESD(h)$). Additional conditioning with a digital elevation model (scenario *h + DEM*) results in a further increase of the mean log-transmissivity and decrease of the recharge rate values. Conditioning to a digital elevation model prevents the model from calculating locally excessive piezometric head values. As a consequence, the uncertainty of the calculated hydraulic head values, as measured by the $AESD(h)$, is strongly reduced. Altogether, the recharge rate is modified less (reduction by a factor of 3) than the transmissivity (increase by a factor of 15) as it is more constrained by the available information.

[51] In scenario *RS*, satellite information is used to constrain the recharge rate estimates further. In this scenario no information on hydraulic head values was used, so that we have to compare it to scenario *basis*. With respect to scenario *basis* the mean recharge rate is reduced, which indicates that the chloride measurements were taken at locations with an enlarged recharge rate (as compared with the average recharge rate over the domain). The RS data also reduce the uncertainty of the spatially variable recharge rate: $AESD(R)$ is reduced from 12.8 mm a^{-1} to 9.0 mm a^{-1}. In spite of a lower average recharge rate, a reduced uncertainty of recharge rate, and unchanged transmissivities (as compared with scenario *basis*), $AESD(h)$ is larger than in scenario *basis*. This is due to some extreme realizations and points again to the fact that 100 realizations are not sufficient to get a stable estimate of $AESD(h)$.

[52] In scenarios *RS + DEM*, *RS + h*, and *RS + h + DEM* the RS data are used together with information on piezometric head values in the conditioning process (see Table 1). If scenario *RS + h* is compared with scenario *h*, and scenario *RS + h + DEM* with scenario *h + DEM* (the difference between those cases being only the use of RS data as conditioning information), the following is observed:

[53] 1. The ensemble standard deviation of the recharge rate is lower if RS data are used for conditioning. Even if hydraulic head data and a digital elevation model are also used as conditioning data, the RS data still yield a considerable uncertainty reduction for the estimation of the recharge rate (3.3 mm a^{-1} in scenario *RS + h + DEM* instead of 8.0 mm a^{-1} in scenario *h + DEM*).

[54] 2. On the other hand, adding RS data hardly changes the ensemble mean and the spatially averaged recharge rate, in comparison with the cases in which also information on the piezometric heads (or the DEM) was used in the inverse modeling. Particularly interesting is the comparison of the results for scenarios *h + DEM* and *RS + h + DEM*. For scenario *h + DEM*, where hydraulic head data and a digital elevation model are used as conditioning information (besides transmissivity and chloride data), the calibrated areally averaged recharge rate is 6.5 mm a^{-1}. In scenario *RS + h + DEM*, where RS data are used in addition, the areally averaged recharge rate after inverse modeling is 6.4 mm a^{-1}.

Figure 2. Ensemble average recharge rate (mm a^{-1}) in the Chobe region for scenarios (a) *basis*, (b) *h*, (c) *h + DEM*, (d) *RS*, (e) *RS + DEM*, (f) *RS + h*, (g) *RS + h + DEM*, (h) *RS + h + Patt*, and (i) *RS + h + DEM + Patt*. Scenarios *basis* and *RS* that are not conditioned to head data and DEM have larger recharge rate values, but the satellite information used in scenario *RS* already yielded a decrease in recharge rate as compared to scenario *basis*.

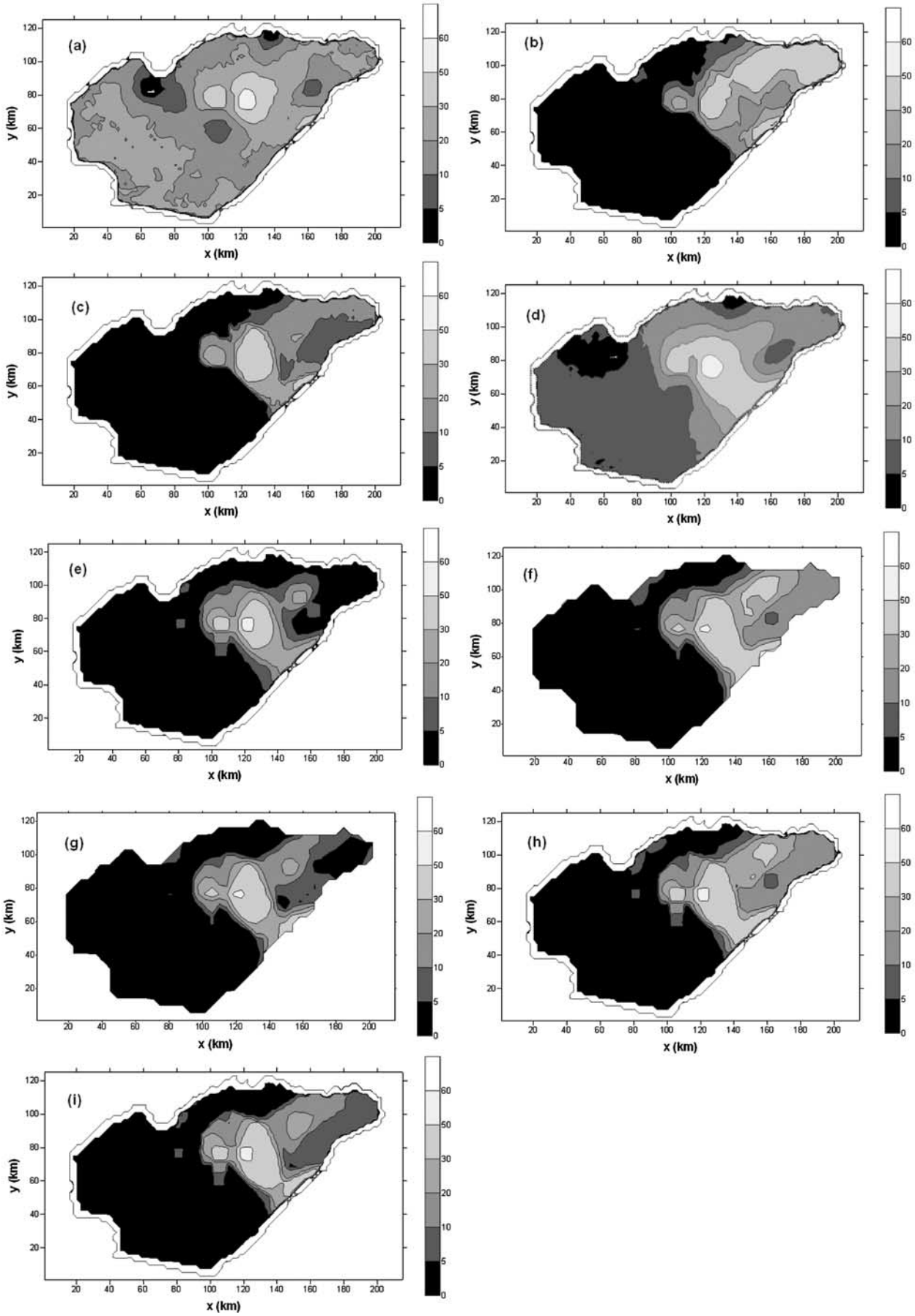

Figure 2

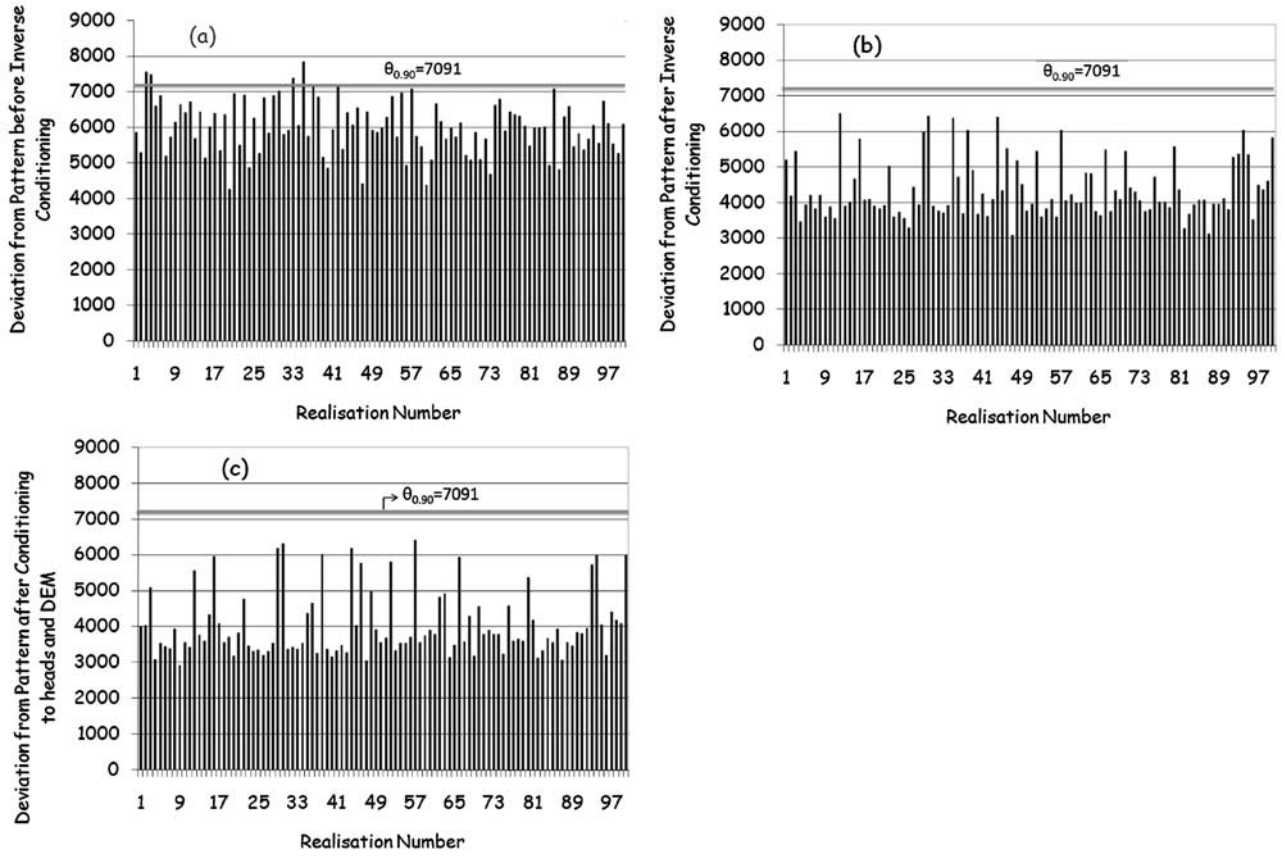

Figure 3. Deviation of the recharge rate pattern, as compared with the remote sensing (RS) image measured in terms of Θ for all the realizations in an ensemble. (a) Before inverse conditioning (scenario *RS*). (b) After inverse conditioning to hydraulic head data (scenario *RS* + *h* + *Patt*). (c) After inverse conditioning to hydraulic head data and a digital elevation model (scenario *RS* + *h* + *DEM* + *Patt*). The ensemble of realizations was in all cases conditioned to transmissivity data, chloride data, and the RS image. The level of $\Theta_{0.90}$ is also indicated.

[55] 3. The ensemble standard deviation of log-transmissivity (*AESD*(*Y*)) increases in scenarios *h* and *h* + *DEM* (as compared with *basis*). It seems that the conditional log-transmissivity realizations are too smooth and that inverse conditioning produces more spatial variability. However, if all data are used for conditioning, including the RS data, the ensemble standard deviation of log-transmissivity is somewhat lower than for scenarios *h* and *h* + *DEM*. This is not a very pronounced effect but could point to the fact that because of the reduced uncertainty of the recharge rates, the uncertainty of the transmissivities is also reduced via the groundwater flow equation.

[56] Finally, for scenarios *RS* + *h* + *Patt* and *RS* + *h* + *DEM* + *Patt*, pattern information is also directly injected into the conditioning. The results are very similar to the ones obtained for scenarios *RS* + *h* and *RS* + *h* + *DEM*. Scenario *RS* + *h* + *DEM* + *Patt* gives slightly larger ensemble variances for transmissivity and recharge rate, compared with scenario *RS* + *h* + *DEM*. The additional conditioning was potentially a problem in deforming individual realizations such that they would differ strongly from the RS image. Therefore the pattern term was added to the objective function. However, additional inverse conditioning to hydraulic head data and DEM yielded recharge rate realizations that were very similar to the RS image, even without including the pattern term. This shows that the initial recharge rate realizations, conditioned to chloride data and RS information by colocated cosimulation, deviated probably too much from the original RS image, based on a too pessimistic perception of the quality of the RS image. In particular, Θ does not give an important contribution to *J*, and during the conditioning this contribution is reduced further, in most cases to zero. Figure 3 shows the Θ values for the 100 recharge rate realizations (generated with colocated cosimulation), before the inverse conditioning (scenario RS), after the inverse conditioning to hydraulic head data (scenario *RS* + *h* + *Patt*), and after the additional inverse conditioning with the digital elevation model (scenario *RS* + *h* + *DEM* + *Patt*). For 99 out of 100 realizations the recharge rate pattern after inverse conditioning to hydraulic head data was closer to the RS image than it was before. This is caused by the conditioning to the hydraulic head data, as the contribution from the perturbation of the RS pattern in the objective function *J* was small. If also the digital elevation model is used as conditioning information, for 88 out of 100 realizations a calibrated recharge pattern was obtained that was even closer to the RS image.

[57] Figure 4 shows some inversely conditioned realizations of recharge rate for scenario *RS* + *h* + *DEM* + *Patt*.

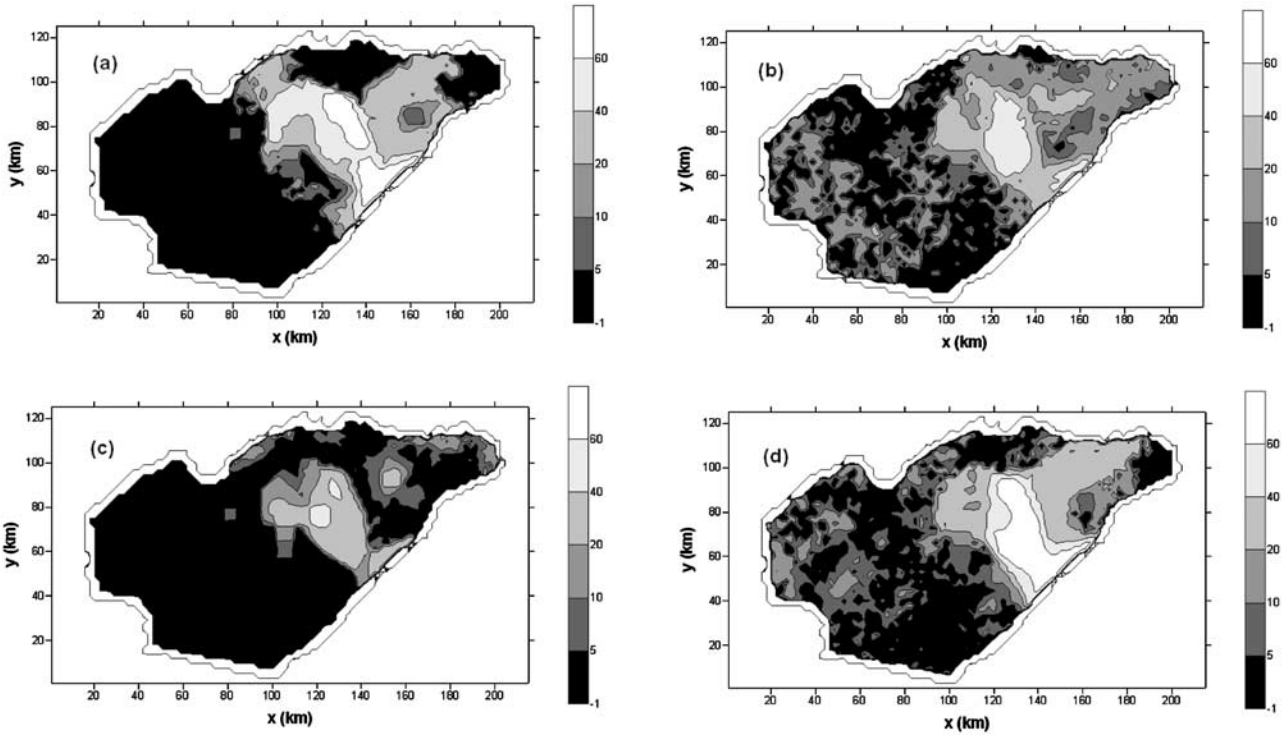

Figure 4. Four realizations of the recharge rate (mm a^{-1}) in scenario *RS + h + DEM + Patt*: (a) realization 26, (b) realization 46, (c) realization 54, and (d) realization 80.

The four realizations display a similar pattern with an area of increased recharge in the eastern, more elevated, part of the study area. Nevertheless, the extent and shape of the area with elevated recharge differ considerably between the stochastic realizations. In two realizations the southwestern part of the Chobe region receives almost no recharge (everywhere less than 5 mm a^{-1}), whereas in the other two realizations the southwestern part also shows large patches with an estimated recharge rate above 5 mm a^{-1}. Figure 5 shows for some scenarios the ensemble standard deviation of the recharge rate and transmissivity. Figure 5 illustrates that including conditioning information in the simulations (as compared with scenario *basis*) reduces the variance of the recharge rate estimate but increases the variance of the transmissivity estimate, indicating that the prior transmissivity variance was too low. The uncertainty of the recharge rate scales with the mean recharge rate (larger uncertainty for higher mean recharge), whereas the transmissivity uncertainty is more evenly distributed over the study area.

[58] It can be concluded that RS information is important for reducing the ensemble variance of inversely conditioned realizations. However, this was merely due to using the RS images for the generation of equally likely recharge rate realizations by colocated cosimulation. Additional constraining of the perturbation of recharge rate realizations during the inverse conditioning procedure, achieved by penalizing too large deviations of the recharge rate realizations with respect to the RS pattern, resulted neither in an additional uncertainty reduction nor in apparent modifications in the estimated values of parameters. Conditioning to hydraulic head data and the DEM (besides the chloride and transmissivity data and the RS image) yields recharge rate patterns that are already close enough to the recharge rate pattern from the RS image. It seems that in this case the pattern information from the RS image does not give additional information about the parameters, which is not yet contained in the other data sources.

6. Additional Analysis

[59] In order to investigate further the potential of including pattern information in the inverse conditioning, some additional analysis has been made. For scenario *h*, where only chloride data, transmissivity data, and hydraulic head data are used for conditioning, the deviation of the recharge pattern Θ (with respect to the RS image) is calculated before conditioning and after conditioning. Before conditioning, Θ was larger than 7091 for all 100 realizations (compare with Figure 3). Analyzing the 1000 recharge rate realizations that are conditioned to chloride measurements and the RS image by colocated cosimulation, one finds a Θ value larger than 7091 for only 10% of the realizations. This illustrates that realizations conditioned only to chloride and transmissivity data have a recharge pattern that is rather different from the RS image. However, additional inverse conditioning to hydraulic head data (scenario *h*) yields for all 100 realizations a reduction of Θ, and after conditioning with heads only 20% of the realizations have a Θ value larger than 7091. This illustrates that hydraulic head data give indirectly important information about the recharge rate pattern for the Chobe region.

[60] The ensemble of 100 realizations for scenario *h*, conditioned to transmissivity, chloride, and hydraulic head data, is analyzed further. The ensemble is split into two groups: a group of 50 realizations with the lowest Θ values

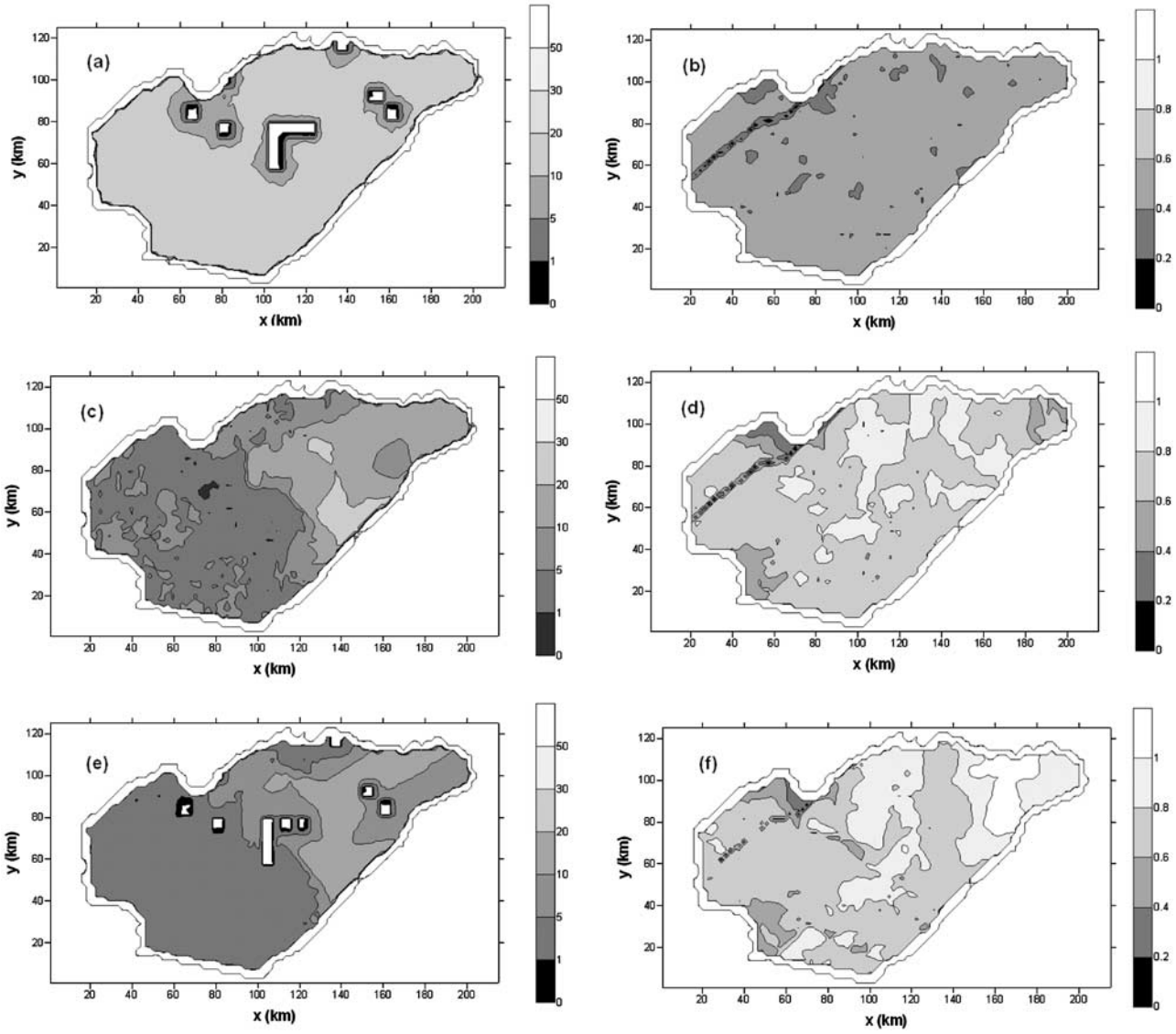

Figure 5. Ensemble standard deviation of (left) recharge rate (mm a^{-1}) and (right) decimal log-transmissivity: (a and b) scenario *basis*, (c and d) scenario *h + DEM*, (e and f) scenario *RS + h + DEM + Patt*.

after inverse conditioning ($\Theta < 4890$), and a group of 50 realizations with the largest Θ values ($\Theta \geq 4890$). For both sets of 50 realizations, ensemble statistics have been calculated (Table 3). It can be seen that the realizations with the lower Θ values have a smaller area-averaged recharge rate (8.8 mm a^{-1}) than the realizations with the larger Θ values (11.0 mm a^{-1}). The lower recharge rate is in better correspondence with the calibrated recharge rate, obtained when all data sources are included in the conditioning. For this particular aquifer the piezometric heads and the recharge rate pattern from the RS image contain similar information. Nevertheless, each information source still has its own value. Using no information on the piezometric head distribution (hydraulic head measurements, DEM) results in too large simulated piezometric head values with too low transmissivities and too large recharge rates. The information on piezometric heads allows us to adjust the absolute recharge rate values. On the other hand, conditioning to chloride data, transmissivity data, DEM and hydraulic head data (scenario *h + DEM*), but not the RS image, yields larger ensemble variances for transmissivity, and especially recharge rate, as compared with the case where also information from the RS image is included (scenario *RS + h + DEM*). We could demonstrate the value of the information contained in the RS pattern, but if all other data sources are used for conditioning, the pattern information does not improve the simulation results further, because the information it carries is already accounted for by the other data sources. However, we believe that for other areas and other case studies, it is important to preserve pattern information in the inverse conditioning. This is especially important if the RS image is more strongly correlated with the variable of interest than in our study. Note that colocated cosimulation includes the pattern information from the RS image, while additional inverse conditioning could "destroy" that pattern information. In that case, pattern information has to be constrained in the inversion. In this study, hydraulic head data and DEM did not "destroy" pattern

Table 3. Evaluation of the Ensemble Statistics for Scenario h[a]

Scenario	Average Y, $\log(m^2\ s^{-1})$	$AESD(Y)$, $\log(m^2\ s^{-1})$	Average R, mm a^{-1}	$AESD(R)$, mm a^{-1}	$AESD(h)$, m
h, *low* Θ	−2.39	0.68	8.8	6.7	217.5
h, *large* Θ	−2.36	0.70	11.0	9.1	174.8

[a]Besides chloride and transmissivity data, only hydraulic head data are used for conditioning. The ensemble statistics are given for the 50 realizations that have a spatial pattern closest to the RS image (low Θ), and the 50 realizations that deviate the most from the RS image (large Θ). Y is log-transmissivity, R is recharge rate, h is hydraulic head, and $AESD$ is average ensemble standard deviation.

information but led to a recharge rate pattern that was more like the RS image, pointing to the fact that probably we were too pessimistic about the quality of the RS image and generated stochastic realizations of the recharge rate that deviated too much from the original RS image. During inverse conditioning, almost all recharge rate realizations that were created on the basis of the RS data became more similar to the RS image. It is very unlikely that this result is incidental; random perturbation of the recharge rate realizations would almost always result in a pattern that would deviate further from the RS image.

7. Conclusions

[61] It can be concluded that nonconventional data sources like, for instance, a digital elevation model or RS images can help to improve groundwater flow models in areas with data scarcity. For the Chobe region considered in this paper, by using a digital elevation model, erroneous artesian piezometric head values could be avoided. In addition, a combination of chloride data and RS data (that are correlated with the recharge rate) strongly constrained the spatial distribution of the recharge rate estimates. In combination with hydraulic head data, this allows us to get an improved estimate of the transmissivities. Without these data sources, the estimated transmissivities could be easily a factor 10 too small, as there were only few transmissivity measurements (all of them with lower values than our calibrated estimate). Still, because a large area is modeled and few data are available, only a global picture of the recharge rate and transmissivity values is obtained. Important uncertainty remains concerning the local hydraulic head or transmissivity values. In addition, given the fact that the limited amount of ground-truth observations (chloride data, hydraulic head data, transmissivity data) was already used for conditioning, no independent data were available for validation. Therefore it was not possible to test more rigorously the impact of the conditioning method described in the paper.

[62] We conclude that RS data are potentially of great value for groundwater flow modeling [e.g., *Brunner et al.*, 2007; *Becker*, 2006]. Especially in areas with serious data scarcity, RS data can help to improve a groundwater flow model and reduce modeling uncertainty. In this study, we focused on two ways to use pattern information from RS in conditioning stochastic inverse models. Further research is needed to develop a more formal methodology for assimilating this kind of information.

[63] **Acknowledgments.** We acknowledge the continuous support of the Department of Water Affairs, Botswana. We remember fondly our project officer Paul Makobo, whose untimely death robbed us of a great colleague and dear friend.

References

Alcolea, A., J. Carrera, and A. Medina (2006), Pilot points method incorporating prior information for solving the groundwater flow inverse problem, *Adv. Water Resour.*, *29*, 1678–1689.

Almeida, A. S., and P. Frykman (1994), Geostatistical modeling of chalk properties in the Dan Field, Danish North Sea, in *Stochastic Modeling and Geostatistics*, *Comput. Appl. Geol. Ser.*, vol. 3, edited by J. M. Yarus, and R. L. Chambers, Am. Assoc. of Pet. Geol., Tulsa, Okla.

Becker, M. W. (2006), Potential for satellite remote sensing of ground water, *Ground Water*, *44*(2), 306–318.

Boni, G., D. Entekhabi, and F. Castelli (2001), Land data assimilation with satellite measurements for the estimation of surface energy balance components and surface control on evaporation, *Water Resour. Res.*, *37*(6), 1713–1722.

Brunner, P., P. Bauer, M. Eugster, and W. Kinzelbach (2004), Using remote sensing to regionalize local precipitation recharge rates obtained from the chloride method, *J. Hydrol.*, *294*, 241–250.

Brunner, P., H. J. Hendricks Franssen, L. Kgotlhang, P. Bauer-Gottwein, and W. Kinzelbach (2007), How can remote sensing contribute in groundwater modelling?, *Hydrogeol. J.*, *15*(1), 5–18.

Capilla, J., J. Rodrigo, and J. J. Gómez-Hernández (1999), Simulation of non-Gaussian transmissivity fields honoring piezometric data and integrating soft and secondary information, *Math. Geol.*, *31*(7), 907–927.

Crow, W. T., and E. F. Wood (2003), The assimilation of remotely sensed soil brightness temperature imagery into a land surface model using ensemble Kalman filtering: A case study based on ESTAR measurements during SGP97, *Adv. Water Resour.*, *26*, 137–149.

Dunne, S., and D. Entekhabi (2005), An ensemble-based reanalysis approach to land data assimilation, *Water Resour. Res.*, *41*, W02013, doi:10.1029/2004WR003449.

Gómez-Hernández, J. J., and A. G. Journel (1993), Joint sequential simulation of multi-Gaussian fields, in *Geostatistics Tróia'92*, volume 1, edited by A. Soares, pp. 85–94, Springer, New York.

Gómez-Hernández, J. J., A. Sahuquillo, and J. E. Capilla (1997), Stochastic simulation of transmissivity fields conditional to both transmissivity and piezometric data: 1. Theory, *J. Hydrol.*, *203*(1), 162–174.

Hendricks Franssen, H. J. (2001), Inverse stochastic modelling of groundwater flow and mass transport, Ph.D. thesis, Tech. Univ. of Valencia, Valencia, Spain.

Hendricks Franssen, H. J., F. Stauffer, and W. Kinzelbach (2004), Joint estimation of transmissivities and recharges—Application: Stochastic characterization of well capture zones, *J. Hydrol.*, *294*(1–3), 87–102.

Herman, A. V., B. Kumar, P. A. Arkin, and J. V. Kousky (1997), Objectively determined 10-day African rainfall estimates created for famine early warning systems, *Int. J. Remote Sens.*, *18*(10), 2147–2159.

Kowalsky, M. B., S. Finsterle, and Y. Rubin (2004), Estimating flow parameter distributions using ground-penetrating radar and hydrological measurements during transient flow in the vadose zone, *Adv. Water Resour.*, *27*, 583–599.

LaVenue, A. M., B. S. RamaRao, G. de Marsily, and M. G. Marietta (1995), Pilot point methodology for automated calibration of an ensemble of conditionally simulated transmissivity fields: 2. Application, *Water Resour. Res.*, *31*(3), 495–516.

Leduc, C., J. Bromley, and P. Schroeter (1997), Water table fluctuations and recharge in semi-arid climate: Some results of the HAPEX-Sahel hydrodynamic survey (Niger), *J. Hydrol.*, *189*(1–4), 123–138.

Lerner, D. N., A. S. Issar, and I. Simmers (1990), *Groundwater Recharge*, *Int. Contrib. Hydrogeol.*, vol. 8, Heinz Heise, Hanover, Germany.

Margulis, S., D. McLaughlin, D. Entekhabi, and S. Dunne (2002), Land data assimilation and estimation of soil moisture using measurements from the South Great Plains 1997 Field Experiment, *Water Resour. Res.*, *38*(12), 1299, doi:10.1029/2001WR001114.

Oliver, D. S., L. B. Cunha, and A. C. Reynolds (1997), Markov Chain Monte Carlo methods for conditioning a permeability field to pressure data, *Math. Geol.*, *29*(1), 61–91.

Reichle, R. H., D. Entekhabi, and D. B. McLaughlin (2001), Downscaling of radio brightness measurements for soil moisture estimation: A four-dimensional variational data assimilation approach, *Water Resour. Res.*, *37*, 2353–2364.

Roerink, G. J., Z. Su, and M. Menenti (2000), S-SEBI: A simple remote sensing algorithm to estimate the surface energy balance, *Phys. Chem. Earth, Part B*, *25*(2), 147–157.

Scanlon, B. R., K. E. Keese, A. L. Flint, L. E. Flint, C. B. Gaye, W. M. Edmunds, and I. Simmers (2006), Global synthesis of groundwater recharge in semiarid and arid regions, *Hydrol. Processes*, *20*(15), 3335–3370.

Seong, K., and Y. Rubin (1999), Field investigation of the Waste Isolation Pilot Plant (WIPP) site (New Mexico) using a nonstationary stochastic model with a trending hydraulic conductivity field, *Water Resour. Res.*, *35*(4), 1011–1018.

Stauffer, F., A. Guadagnini, A. Butler, H. J. Hendricks Franssen, N. van der Wiel, M. Bakr, M. Riva, and L. Guadagnini (2005), Delineation of source protection zones using statistical methods, *Water Resour. Manage.*, *19, 163–185.*

P. Brunner, School of Chemistry, Physics and Earth Sciences, Flinders University, GPO Box 2100, Adelaide, South Australia, Australia 5001.

H. J. Hendricks Franssen and W. Kinzelbach, Institute of Environmental Engineering, ETH Zurich, Wolfgang Paulistrasse 15, CH-8093 Zurich, Switzerland. (hendricks@ifu.baug.ethz.ch)